Proceedings of the ASME 2014 International Design Engineering Technical Conferences & Computers and Information in Engineering Conference
IDETC/CIE 2014
August 17-20, 2014, Buffalo, USA

DETC2014-35539

DESIGN OF A WEARABLE SCISSORED-PAIR CONTROL MOMENT GYROSCOPE (SP-CMG) FOR HUMAN BALANCE ASSIST

Jimmy Chiu*
Honda Research Institute USA, Inc.
Mountain View, California 94043
Email: JChiu@honda-ri.com

Ambarish Goswami
Honda Research Institute USA, Inc.
Mountain View, California 94043
Email: AGoswami@honda-ri.com

ABSTRACT

Our research examines the feasibility of usign a wearable scissored-pair control moment gyroscope (CMG) for human balance assist. The CMG is a momentum exchange device consisting of a fast spinning flywheel mounted on a gimbal. The gimbal motion changes the direction of the flywheel rotation axis, which generates a reactionless torque. A scissored-pair CMG has the additional advantage of isolating the output torque to a single axis, where off-axis torques are canceled out. A properly designed CMG device worn as a backpack can apply a torque in the sagittal plane of the human trunk. This can help in restoring postural balance and in fall mitigation.

This paper describes the complete design process of a scissored-pair CMG device with constraints on size, mass and dynamic properties for human wearability. A prototype of this device is built, utilizing a novel dual-flywheel design; it weighs about 8kg and is able to generate over 20Nm of torque. A custom hardware is built specifically for verifying the torque output of the device. To our knowledge this is the only device that generates the range of reactionless torque given its weight and size.

INTRODUCTION

Reactionless actuators such as Control Moment Gyroscopes (CMG) and inertia wheels [1] are able to apply actuation torques through the exchange of angular momentum without requiring external forces acting on the body. Such devices have traditionally been employed to control the attitude of satellites, boats and submersible vehicles [2, 3]. We envision the use of such devices in applications of balance assist for humans. Figure 1 shows the prototype device that we have designed and built (left), which can be worn as a backpack (right).

FIGURE 1. Left: A scissored-pair CMG prototype. Right: The same device worn as a backpack.

Most of the existing commercially available products are not fit for human wearability due to their excessive mass or insuffi-

*Address all correspondence to this author.

Copyright © 2014 by ASME

cient torque. They are geared towards the control of large satellites with masses of up to 1000kg (e.g. Honeywell M50 [4], Astrium 15-45S [5]) or significantly smaller cubesats with sub 10-kg masses (Honeybee TORC [6]). However, these applications have unique requirements of being able to withstand the conditions of space, thereby significantly increasing their mass and cost. Even larger CMGs designed for ship stabilization (e.g. Seakeeper M-series [7]) are also commercially available. A schematic overview of some existing CMGs is shown in Figure 2; commercially existing products fall in the ranges applicable for Cubesats/Nanosats, large satellites and ships. However, none of the devices shown in the range applicable for human assist (up to 10kg, 0.5-50Nm) exists commercially, as each of these proposed or actual prototypes are custom designs. Note that some are proposed but not known to have actually been built. Proposed designs by the authors of [8–10] are shown as examples of devices satisfying the applicable range of mass and torque for human assist, along with the prototype design for our SP-CMG outlined in this paper.

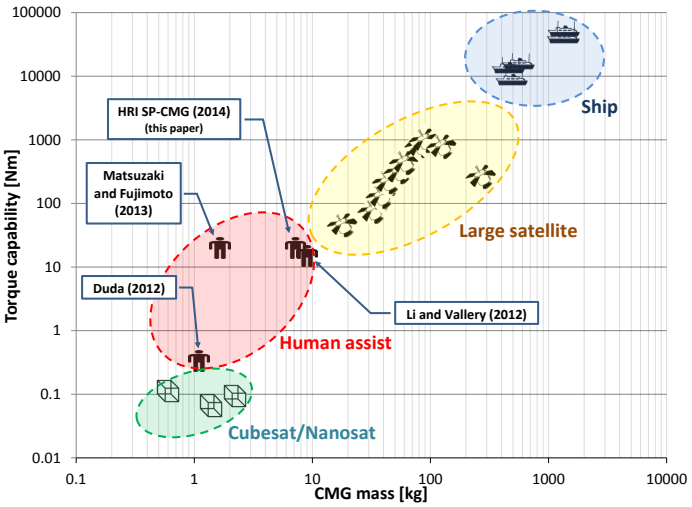

FIGURE 2. Mass and torque ratings plotted on log-log scale for existing CMG devices of various categories. A number of commercially existing CMGs for Nano and Cubesats, large satellites and ships are included, obtained with data taken from [11] and product datasheets. These devices are primarily made for re-orienting satellites or for the stabilization of boats and submarines. However, no commercially available CMGs exist in the defined "Human assist" range, given by a torque range of 0.5-50Nm and a total mass lower than 10kg. A few custom-built prototypes, where such mass and torque capabilities would be useful for human assistance devices, have been built or proposed [8–10]. These are shown in the human assist range along with our prototype outlined in this paper.

Recent research has shown that wearable reactionless actuators can be a viable option to assisting humans for balance recovery [8–10, 12], however the devices used in these research projects are custom-designed and fabricated parts that are not commercially available. A full body suit consisting of several CMG modules is proposed in [8] as a method of assisting humans in adapting to microgravity conditions in space by providing a sense of "down" and also generating viscous resistance during movement to prevent muscle atrophy. In this bodysuit the CMG flywheels are 58grams each and spinning at approximately 1000rpm, however torque output levels are sub-Nm, which is not sufficient for human balance assistance.

Simulations reported in [9] show the feasibility of human balance assist using CMGs, where output torques are under 15Nm. In this study, the system consists of three CMGs, where each flywheel mass is assumed to be 2500grams spinning at 9000rpm. The authors of [10] also propose a CMG to aid in human balance, where the flywheels are 500grams, spinning at up to 19000rpm, with output torques are up to 20Nm. In fact, the proposed devices in both [9] and [10] would fall into the 'Human assist CMGs' space in Figure 2.

The use of such devices in the field of human assistance or human augmentation is of particular interest because it opens up the possibility of providing support or haptic feedback [13–15] to the wearer without requiring any ground contact. The wearable devices can therefore be completely isolated and self-contained and can be used without the restriction of being tethered to the physical environment.

By having control of torques acting on the human, it is also possible to design active controllers to improve balance and stability in difficult situations such as balancing on a narrow beam [12]. One can envision the use of such devices not only in assistive applications, but even enabling humans to perform tasks such as re-orientation in mid-air.

Following the work of Li and Vallery [9] and Matsuzaki and Fujimoto [10] it has been shown that this novel use of reactionless actuators for human assist opens up a variety of new possibilities not realizable with traditional actuators. Our intent is to investigate the efficacy of using wearable reactionless actuators to mitigate the fall of a human, focusing on reducing or eliminating the falling motion in the sagittal plane. The human-fixed coordinate axes and the accompanying planes of motion are shown in Figure 3.

WORKING PRINCIPLE OF A CMG

A basic type of reactionless actuator is an inertia wheel, where the angular momentum due to a spinning flywheel is exchanged from the spinning wheel to the body it is attached to. The inertia wheel and the attached body satisfy the conservation of angular momentum, thus the momentum exchange, or transfer of angular momentum, is done by slowing down the flywheel and

Copyright © 2014 by ASME

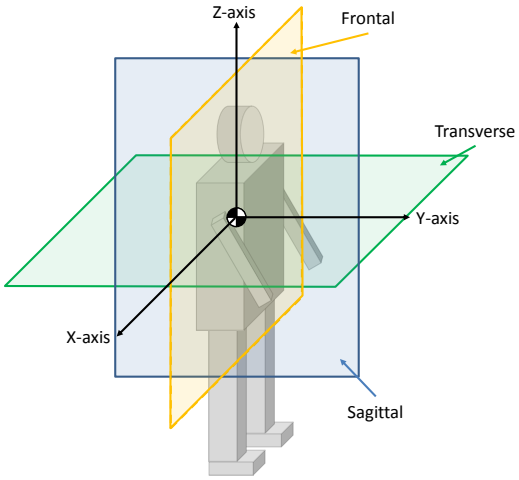

FIGURE 3. Motion of the human is in the sagittal, transverse and frontal planes, with accompanying x, y and z axes. Our goal is to generate a torque about the x-axis, such that the motion in the sagittal plane during loss of balance is reduced.

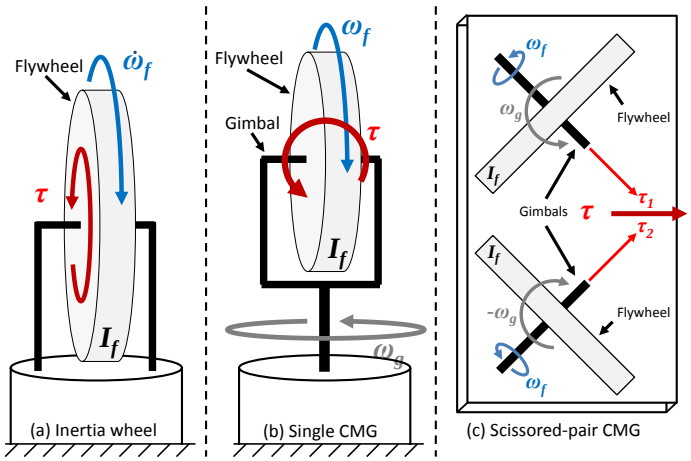

FIGURE 4. (a) An inertia wheel generates a output torque due to the change in angular velocity of the flywheel $\dot{\omega}_f$. (b) A single CMG consists of a rotating flywheel with moment of inertia I_f mounted on a rotating gimbal. The output torque is generated due to the rotation of the gimbal, and the magnitude of the torque is proportional to the angular velocities of both the flywheel and the gimbal. (c) The scissored-pair CMG consists of two identical CMGs having equal flywheel inertias and angular velocities. The gimbals are rotated in opposite directions such that the two output torques add up in the sagittal plane but cancel each other out in the transverse plane.

accelerating the body [16]. The overall angular momentum of the combined system (inertia wheel plus body) is constant, however the angular momentum is transferred between both bodies due to acceleration and deceleration of the flywheel. Note that in the case of an inertia wheel, the direction of the angular momentum remains in a fixed by the orientation of the flywheel, thus the torque due to change in angular momentum (by acceleration or deceleration of the flywheel) are also fixed in the same direction, shown in Figure 4(a).

A CMG is basically an inertia wheel mounted on an actuated gimbal, as shown in Figure 4(b). The primary benefit of a CMG over an inertia wheel is that the output torque is proportional to both the flywheel angular velocity and the angular velocity of the gimbal, thus allowing for larger output torques than the torque required to spin the gimbal (this property is known as "torque amplification" [17]). This provides a great advantage of being able to provide large output torques without the necessity of large actuators. The torque output from the CMG is given by the cross product of the angular momentum of the flywheel ($I_f\ \omega_f$) and the angular velocity of the gimbal (ω_g), as expressed below:

$$\tau = I_f\ \omega_f \times \omega_g \tag{1}$$

where I_f is the moment of inertia of the flywheel, ω_f is the angular velocity of the flywheel. The direction of the output torque is given by the cross product of the flywheel spin axis and the gimbal rotation axis. As the direction of the gimbal axis changes, so does the output torque direction.

From Equation 1 we can see that the output torque τ is proportional to the flywheel moment of inertia $I_f\ \omega_f$, the flywheel speed ω_f and the gimbal speed ω_g. The moment of inertia of the flywheel is inherently tied to its size and mass, whereas we can increase torque output for a given size/mass by increasing the flywheel speed. Increasing gimbal speeds also increases the output torque magnitude, however the output torque direction also changes faster. Therefore if the goal is to increase torque in a particular direction, the gimbal speed becomes a tradeoff between applied torque magnitude and duration.

Scissored-pair CMG Since our objective is to provide a torque in the sagittal plane there are two potential methods that can be utilized to isolate the torque about the single axis. First, we can limit the gimbal angle such that the cross product of the flywheel rotation and gimbal axes result in a torque about the sagittal plane, however transverse torque increases as the range of gimbal motion increases. The second approach is to utilize the so-called **Scissored-Pair CMG** [18], which consists of a synchronized pair of identical CMGs which are rotated in opposite directions, as shown in Figure 4(c). Thus torques from the two CMGs add up in the sagittal plane and cancel each other in the transverse plane. The result of the scissored-pairing is that the net output torque is about a fixed-axis, though its magnitude is varying. In Figure 5 we show schematically the output torque of each individual CMG in the scissored-pair in the sagittal plane (Figure 5 (a)) and transverse plane (Figure 5 (b)). The combined outputs

Copyright © 2014 by ASME

of the scissored-pair for each plane are shown in Figures 5 (c) and (d). Note that we can eliminate the transverse torque by synchronizing the scissored-pair, or add transverse torque by designing the gimbal motion profile such that they are non-synchronous.

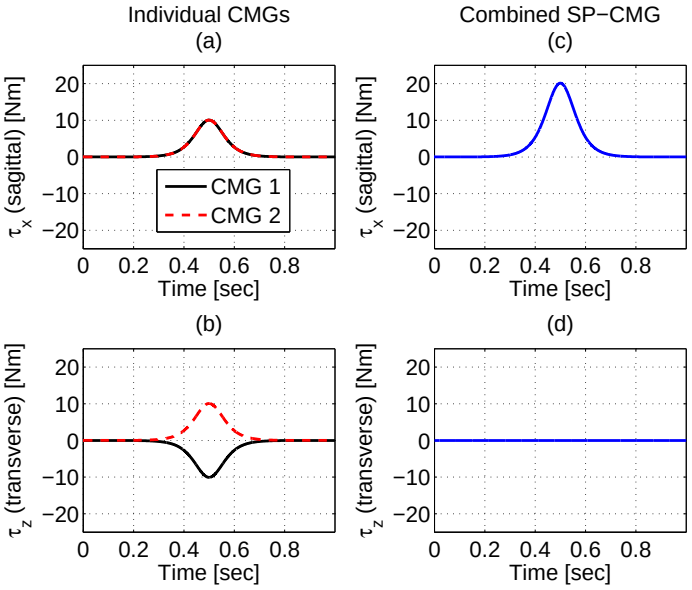

FIGURE 5. A scissored-pair CMG adds the torque outputs of the individual CMGs in the intended (sagittal) plane and cancels them in the transverse plane. Because the gimbals and flywheels have the same speed (but opposite directions) output torque of the individual CMGs in the sagittal plane are equal in sign and magnitude (shown in (a)), and in the transverse plane are equal magnitude but opposite sign (shown in (b)). This results in an output of double the magnitude in the sagittal plane (Figure 5 (c)), and a zero torque profile in the transverse plane (Figure 5 (d)). In this example, the gimbal speed is determined by the derivative of a sigmoid function through a range of 90°, shown in Figure 10.

If we continue to rotate the two CMGs in the scissored-pair such that the gimbals complete their full revolution, the resulting torque direction completes a 360° rotation also. Therefore the torque about the x-axis will be negative when the gimbal is rotated beyond 180°. The negative portion of the sagittal plane torque will effectively push the trunk away from the safe upright orientation. Therefore, we rotate the gimbals for only half a revolution which corresponds to the "positive" torque. After which they must be brought back to the start configuration in order to be ready for the next activation. So that the gimbals can be reset without generating too much torque, they are rotated back with a much lower angular velocity, assuming that the lower magnitude torque over a longer duration would not induce instability. Since the magnitude of the output torque is proportional to the gimbal angular velocity ω_g, the slow motion of the gimbals during the reset phase and the resulting low magnitude torque should be unnoticeable by the wearer.

DESIGN REQUIREMENTS

Our initial approach is to provide assist in the sagittal plane, assuming that loss of balance occurs most frequently in this plane. However, the proposed design can be extended for multi-plane fall mitigation with the modification of the CMG gimbal motion profiles.

To determine the necessary sagittal plane torque for human balance assist, we consider a simple single degree-of-freedom inverted pendulum model of the trunk mass rotating at the hip. In this approach we determine the necessary torque applied at the hip to hold the trunk at various lean angles ϕ. It is assumed that the trunk mass is 43.5kg (approximately 50% of total mass [19]), with a trunk center of mass 0.45m above the hip joint [20] (i.e. the length between the rotation axis and trunk center of mass). The torque (τ_ϕ) required to support 50% of the mass at static equilibrium with a trunk lean angle of 15° is 25Nm, shown in Figure 6. In this device the goal is not necessarily to provide 100% of the torque required to support the trunk leaning at a fixed angle since it is naturally supported by the muscles. The primary task is to have sufficient torque such that the combined torque from the CMG and the muscles causes an angular deceleration of the trunk during the fall.

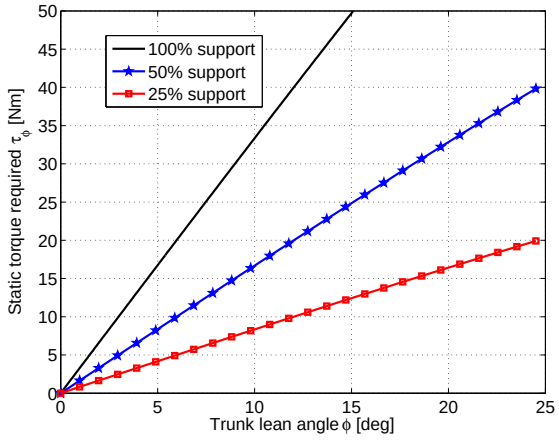

FIGURE 6. The torque required to statically support the torso about the hip joint increases with the trunk lean angle. The required torques for 100%, 50% and 25% of the trunk mass are shown for lean angles up to 25°.

With a trunk moment of inertia of 11.7kgm^2 in the sagittal plane [20], the 25Nm torque from the CMG results in an angular

Copyright © 2014 by ASME

deceleration of $122^\circ/s^2$. Measured trunk angular accelerations for a typical fall are a magnitude lower, at less than $17^\circ/s^2$ [21], thus the generated torque from the CMG has the potential to not only decelerate the fall, but also counteract it and cause the trunk rotation to be reverted.

One of the limitations that needs to be considered for a wearable device is the effect on gait due to carrying additional mass. In [22] the authors demonstrate that an additional 6kg of mass added to the human pelvis does not cause a discernable change in the gait. Furthermore, the authors find no change in metabolic rate for walking when an inertia equivalent to a 10kg load is applied to the pelvis. Following this, our mass constraint for the wearable device is chosen to be 10% of the average total human mass, approximately 8.7kg [19].

MECHATRONIC HARDWARE DESIGN OF THE CMG

Our main design objective is to develop a CMG system that can generate a 25Nm torque. In addition, the device needs to be light, not more than 9kg, to allow for wearability. Furthermore, it must be safe in case of a catastrophic failure of any of the components.

The three main mechanical elements of the CMG are the flywheels, the gimbals and the chassis. Additionally, the design process involves motor selection as well as the design of the associated electronic circuitry to support the motion requirements. The section drawing of the CMG assembly is shown in Figure 7. Below, we describe the design of the components and the entire system assembly one by one.

Flywheel Design In order to limit the size of the device as well as the amount of overhang from the back of the subject, we set the flywheel radius to 50mm. From the design constraints of torque, mass and size, it is possible to demonstrate that there is a feasible design space with the flywheel radius of 50mm, with the size constraint being the primary design constraint. In Figure 8 we demonstrate a feasible design space that satisfies the spatial, mass and torque requirements of the device. Here, each of the four flywheels (two gimbals for the scissored pair, using the dual-flywheel gimbal design shown in Figure 7) are limited to 900grams, resulting in a total flywheel mass of 3600grams.

Ideally, the flywheel should be designed with the mass located at the maximum radius (i.e. at the outer perimeter) to maximize the rotational moment of inertia, however for this initial prototype we have chosen to keep the flywheel design as a simple solid disk with a center bore for easier analysis of the mechanical properties.

For the solid disk, the mass is given by:

$$m_f = \pi r^2 t \rho \tag{2}$$

where r is the flywheel radius, t is the thickness and ρ is the material density. The moment of inertia of a thin disk (i.e. the flywheel) about its spin axis is given by:

$$\begin{aligned} I_f &= \frac{1}{2} m r^2 \\ &= \frac{\pi}{2} r^4 t \rho \end{aligned} \tag{3}$$

To increase the moment of inertia for a given size, we choose a material with high density and high strength. The selected material satisfying the desirable properties is an alloy of tungsten (ASTM B777), with a density of $18.5 g/cm^3$ and a yield strength of 600MPa. From Equations 2-3 we can see that both mass and moment of inertia of the flywheel vary linearly with thickness and material density. That is, for a fixed radius we can either increase thickness or density without any difference in mass or moment of inertia. However, everything else remaining same, a higher density will allow us to use a more compact flywheel, and hence a more compact overall package.

For this simple bored disk, the radial and tangential stresses on the rotating flywheel also limit the amount of angular momentum from the CMG. In Figure 9 we show that the peak stress acts in the tangential direction at the center bore. Any failure of the flywheel could be catastrophic as the angular velocities are large,

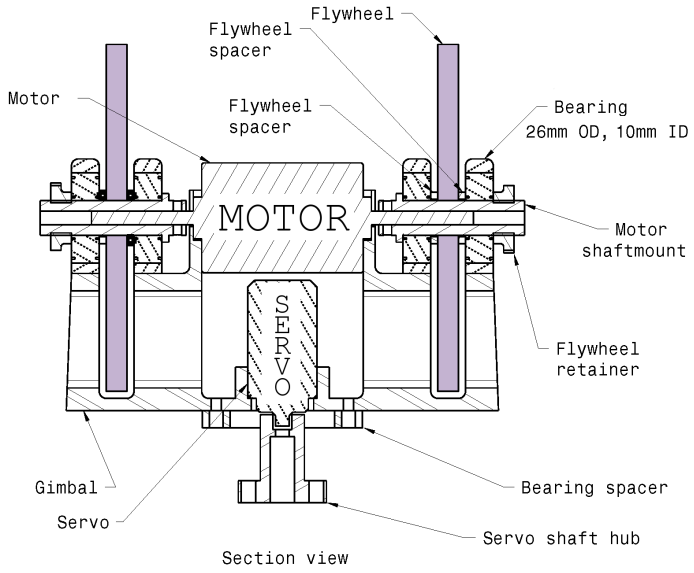

FIGURE 7. Section drawing for each CMG showing the flywheel loads supported on the bearings on each side. The gimbal features an unique dual-flywheel design which balances the masses about the gimbal spin axis. The generated output torques are not transmitted through the motor output shaft back to the gimbal, but are directly transmitted through the bearings. Two of such CMGs are operated in a scissored-pair to make up the CMG.

Copyright © 2014 by ASME

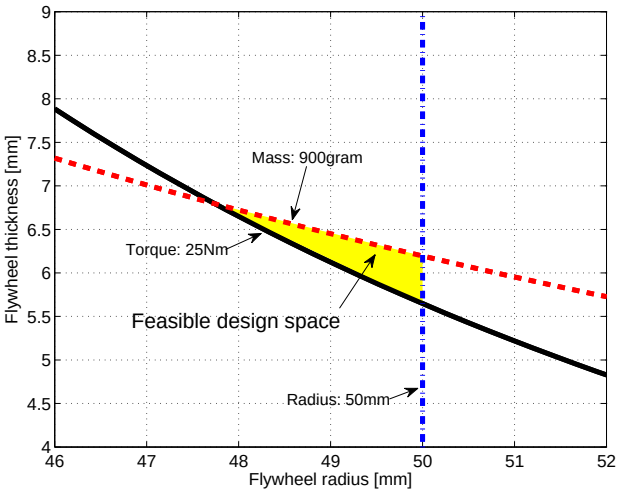

FIGURE 8. There exists a feasible design space satisfying the size, torque and mass constraints of the wearable CMG device, shown in the shaded area. Torque output is constrained by a minimum of 25Nm at a flywheel speed of 5000rpm (above the curve is feasible). The size restriction is driven by a maximum flywheel radius of 50mm (left of the vertical line is feasible), and the mass constraint is 900grams per flywheel (below the curve is feasible).

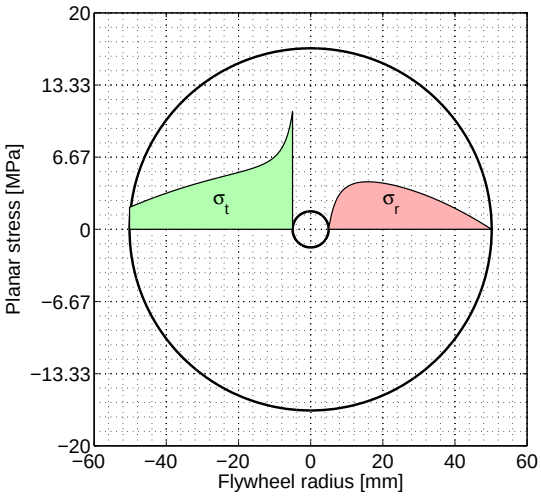

FIGURE 9. Radial (σ_r) and tangential (σ_t) stresses on the flywheel as a function of radius, calculated for a flywheel angular velocity of 5000rpm. The resulting peak stress of 10.87MPa occurs at the center bore in the tangential direction.

thus the yield stress of the flywheel material must exceed this peak stress with some safety margin. In this case, the peak stress of 10.87MPa is over 55 times lower than the yield strength of the tungsten alloy that we used. In theory, speeds of up to 16500rpm could be achievable even while maintaining a safety factor of 5, however in the initial prototype we limit the flywheel to 5000rpm to account for the lack of dynamic balancing.

Gimbal Design Because the flywheel needs to be rotated in order to generate a torque, the primary driving dimension of the CMG device is determined by the flywheel radius. Unlike an inertia wheel, where motion is constrained to a single plane, the CMG needs to account for the swept volume of the flywheel assembly as the flywheel and gimbal rotate about the gimbal axis. In order to increase the moment of inertia of the flywheels without increasing the radius, it is necessary to make the flywheel thicker (and thus heavier). However this approach results in having a potentially unbalanced gimbal, or requiring counterbalances. In order to balance the gimbal rotation whilst satisfying the larger flywheel mass, we designed a dual-flywheel CMG, in which a centrally locate motor contains two identical flywheels mounted on each side of the motor shaft. In this configuration each flywheel can be only half as thick as the required total thickness.

To reduce vibrations and stresses on the rotating flywheel shaft, it is supported by low friction bearings on either end. The section drawing of the CMG assembly shown in Figure 7 shows the two mounted bearings each side of each flywheel. The assembly is designed such that the motor shaftmount on each side holds both bearings, flywheel spacers and the flywheel as a single sub-assembly, secured by the flywheel retainer. The motor output shaft is coupled to the flywheel through set screws on the motor shaft mount, only providing torque to accelerate the flywheels. Output torque generated by actuation of the CMG is directly transferred from the rotating flywheel to the gimbal as the bearing housings are rigidly fixed to the gimbal. The output torque from the flywheel is directly transferred to the gimbal through the bearings, thus the motor output shaft does not carry any of the large torques which would otherwise bend the shaft.

Chassis/Safety The two gimbals comprising of the CMG are positioned in line vertically to allow for a slender and tall chassis for the wearable device. Since the design is for a wearable backpack, the narrow profile on the back reduces restriction in twisting or turning motion of the wearer. The CMG chassis backplate is 5mm thick 7075-T6 aluminum for high strength and lightweight in order to account for the safety of the wearer in case of catastrophic failure of the high speed flywheels. The CMG is attached to the wearer through a four-point harness, going over the shoulders and around the waist to provide a secure and rigid connection with the wearer.

The entire CMG is enclosed with a 3mm carbon-kevlar case/shield to ensure safety of the wearer or others if catastrophic failure occurs, even though a large safety factor is already accounted for in the design of the flywheels. The case weighs 850grams, whereas the same component made out of 3mm thick steel would be over 3.7kg.

Copyright © 2014 by ASME

Motor Selection In order to use symmetrically mounted dual-flywheels per gimbal, we need a motor that has output shafts on both ends of the motor body. A KinetiMax32 EB dual-shaft motor is selected for its lightweight and compactness properties. The motor has a built in tachometer and closed loop speed controller to ensure that the flywheels are spun at precise speeds, which is necessary for the scissored-pair. The motors weigh in at 260grams (for the pair) and is capable of driving the flywheels to a torque-limited 5000rpm.

Off-the-shelf high speed and high torque servos (Hitec HS-8380TH) are utilized for the gimbal motor, with a maximum torque output of 3.5Nm. Each servo is housed inside the gimbal and the torque is applied to the chassis through a spline gear. Initial tests of the gimbal servos with a single step command for the rotation identified one of the flaws in the design, where the servo gears were being damaged by the large decelerations caused when the gimbal reached its final position.

In order to reduce the stress on the servo geartrain, the rotation angle profile was modified to utilize a translated sigmoid function such that the accelerations at the beginning and end of the motion were reduced. The maximum slope of the sigmoid function is set to meet the maximum specifications for the servo. The commanded servo position profile is shown in Figure 10, utilizing the sigmoid gimbal position profile for actuation, followed by a linear reset profile at a reduced speed.

The peak gimbal rate for actuation is 267°/s, whereas the reset is completed at a constant -44°/s, resulting in significantly lower negative torques during the reset profile.

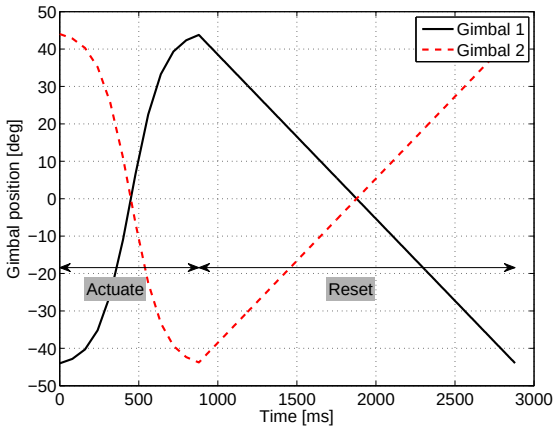

FIGURE 10. Gimbal position command profile for actuation (generation of fall mitigation torque) using a sigmoid function profile and linear gimbal reset profile. The actuation phase is 880ms, whereas the reset is 2000ms, resulting in maximum angular rates of 267°/s and -44°/s, respectively.

Parts	Material	Mass [grams]
Flywheels (4)	Tungsten	3600
Gimbals (2)	Aluminum/Steel	1100
Chassis (1)	Aluminum	650
Safety cover (1)	Carbon-kevlar	850
Microcontrollers (1)	-	120
Motors/Servos (4)	-	400
Batteries (2)	Li-Ion/Ni-MH	980

TABLE 1. Component masses in the CMG prototype listed by parts. The masses are listed for the total number of required parts in the assembly, not for each individual part.

Electronics The control of the flywheel and gimbal motors are done using an Arduino microcontroller, where the activation of the CMG is performed manually using a handheld trigger. Position commands are issued to the gimbal through pulse width modulated (PWM) outputs, with each servo receiving its own command to allow for individual calibrations. The gimbal motion profiles are pre-programmed into the Arduino and played back when the activation trigger is depressed. In the future, we plan to incorporate IMUs into the system in order to implement an automatic trigger algorithm. Multiple gimbal motion profiles could be stored in a lookup table and selected based on the fall signals measured from the IMU.

Power is supplied to the CMG through two battery packs. A primary 87Wh capacity lithium-ion pack supplies the two flywheel motors (at 24VDC) and the Arduino Uno microcontroller (at 9VDC). The secondary 7.2V Ni-MH battery drives the gimbal servos.

TORQUE OUTPUT VERIFICATION

In order to measure and confirm that the hardware generates the amount of torque expected from the theoretical analysis we built a measurement plate consisting of a ball joint and two load cells. In this approach we are able to measure two axes of torque acting on the CMG to determine the sagittal and transverse torques generated during the actuation of the gimbal. The CMG is placed on the measurement plate in such a way that its longitudinal mid-line coincides with the diagonal line of the plate, which bisects the line connecting the two load cells. A schematic of the measurement plate with the load cell width dimension d_w and length from the ball joint L_s is shown in Figure 11. The experimental setup is shown Figure 12.

Once the CMG is rigidly attached to the measurement plate, any torques from the CMG can be measured by knowledge of the load cell position relative to the ball joint. By looking at the change in the force data we can effectively calculate the torque

Copyright © 2014 by ASME

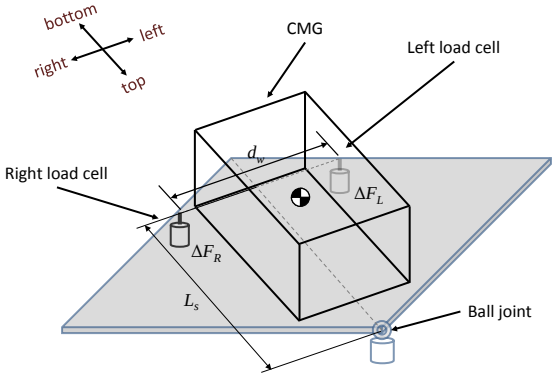

FIGURE 11. A hardware set up to experimentally measure the torque generated by the CMG device in both sagittal τ_x and transverse τ_z planes. The set up uses two load cells attached to a stiff rectangular metal plate, one corner of which is connected to the ground through a free ball joint. Note that the top-bottom-left-right arrows in the top left corner of the figure correspond to the human wearing the device.

in both sagittal (τ_x) and transverse planes (τ_z) by the following relationships:

$$\tau_x = L_s\left(\Delta F_L + \Delta F_R\right) \tag{4}$$

$$\tau_z = \frac{d_w}{2}\left(\Delta F_L - \Delta F_R\right) \tag{5}$$

In Figure 13 we show the measured torque output for various flywheel speeds (1000, 2000, 3000, 4000 and 5000rpm), using the same gimbal control profile. Both sagittal (τ_x) and transverse (τ_z) torques are measured to demonstrate the rise in output torque as flywheel speed (and thus angular momentum) is increased. At 1000rpm, a maximum of 3Nm of torque is generated, increasing to a maximum of 20Nm at 5000rpm. Theoretically the increase in peak torque should be linearly proportional to the flywheel speed, however the experiments show more than expected torque at 5000rpm as the gimbal rotation is slightly quicker. Torque during the 'Reset' phase is significantly lower due to the lower gimbal rate, resulting in negligible negative torque in the sagittal plane. Transverse torque output is limited due to the scissored-pair motion of the CMGs, however because the gimbals are not exactly synchronized, there is a short duration at the end of the gimbal motion where less than 2.5Nm of transverse torque is generated.

It is worth noting that the vibrations from the flywheel are also picked up on the load cell measurements. Recall that no dynamic balancing was done on the manufactured parts, resulting in increasing vibrations as the flywheel speeds were increased. However the high frequency nature of the vibrations (resonant frequency of about 46Hz) result in torque that would be attenuated by the larger mass of the wearer of the device.

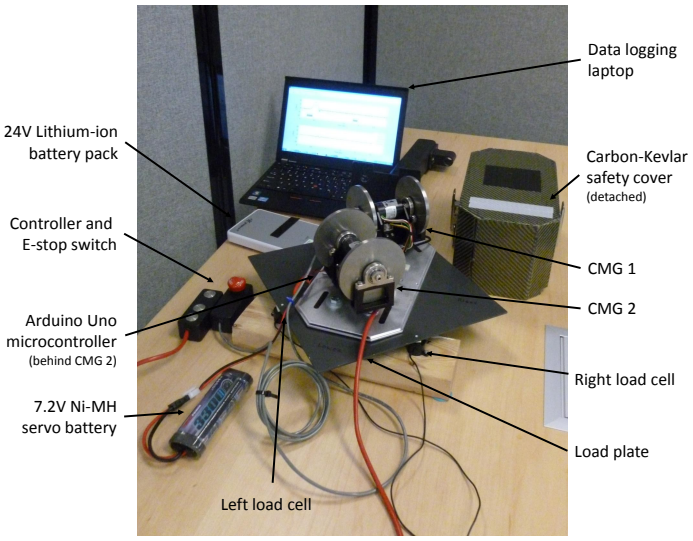

FIGURE 12. Experimental setup on the torque measurement plate with the Carbon-Kevlar safety cover detached. The 24V lithium-ion battery supplies 24V for the flywheel motors as well as 9V for the Arduino control board, occluded by CMG 2. A separate 7.2V Ni-MH battery is used to supply voltage to the servos.

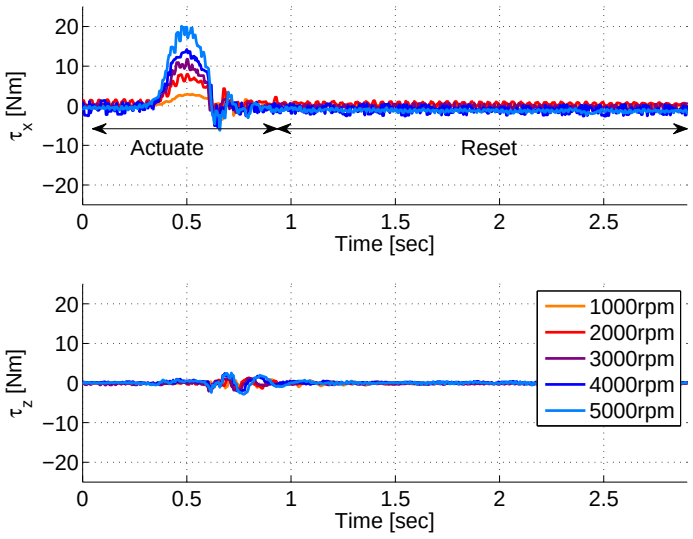

FIGURE 13. Sagittal τ_x and transverse τ_z torques measured at various flywheel speeds (rpm). The transverse torques τ_z are significantly lower than the sagittal torques τ_x due to the scissored-pair motion of the gimbals.

CONCLUSIONS

In this work we have demonstrated the feasibility of using CMGs as a potential wearable balance assist device for humans. Based on the current design of the CMG it is possible to gen-

Copyright © 2014 by ASME

erate torque magnitudes sufficient to affect the motion of a human such that the falling motion is delayed sufficiently to allow for more time to regain balance. There are several options that can be used in the next iteration of the device to obtain larger torque outputs or reduce the overall mass of the backpack. For example, in subsequent designs we can optimize the flywheel for higher rotational moment of inertia without any additional cost in mass by using a spoked wheel design. However, a finite element analysis may be required to identify the stress distribution of the rotating flywheel. By increasing the flywheel speeds or increasing the moment of inertia of the flywheels it is possible to further increase the angular momentum of the CMG, without increasing the mass and size of the device.

For now, our device is activated by an external trigger, however we will add additional sensors and a fall detection algorithm to automate the actuation of the CMG for fall mitigation. Further work needs to be done in human trials to determine what torque output profiles are desirable based on the severity of fall, whether it is more efficient to provide a large peak torque over a short duration, or a lower peak torque for a longer duration, by modifying the gimbal motion profile. We will also investigate the possibility of independent gimbal control to create transverse torques in the event that the fall is not purely in the sagittal plane. The transverse torque can be generated by adjusting the velocity profile of the individual gimbals, however the exact timing of the transverse torque will need to be investigated.

ACKNOWLEDGMENT

Ambarish gratefully acknowledges fruitful discussion with Heike Vallery of Delft University of Technology, Netherlands.

REFERENCES

[1] Block, D. J., Åström, K. J., and Spong, M. W., 2007. *The Reaction Wheel Pendulum*. Synthesis Lectures on Control and Mechatronics. Morgan & Claypool Publishers.

[2] Sidi, M. J., 1997. *Spacecraft Dynamics & Control*. Cambridge University Press.

[3] Thornton, B., 2006. "The development of zero-g class underwater robots: Unrestricted attitude control using control moment gyros". PhD thesis, University of Southampton, Southampton, UK.

[4] Honeywell International Inc., 2006. M50 Control Moment Gyroscope. http://www51.honeywell.com/aero/common/documents/myaerospacecatalog-documents/M50_Control_Moment_Gyroscope.pdf. [Online; accessed 01/27/2014].

[5] Astrium, 2012. CMG 15-45S. http://www.astrium.eads.net/media/document/astrium_gnc6_mdef.pdf. [Online; accessed 01/27/2014].

[6] Honeybee Robotics, 2013. MicroSat Control Momment Gyroscope Array. http://www.honeybeerobotics.com/wp-content/uploads/2013/12/Honeybee-Robotics-Tiny-CMGs.pdf. [Online; accessed 01/27/2014].

[7] Seakeeper Inc., 2013. M8000 Specifications. http://www.seakeeper.com/products_m8000_specifications.php. [Online; accessed 02/21/2014].

[8] Duda, K. R., 2012. "Variable vector countermeasure suit (V2Suit) for space habitation and exploration". NIAC Phase I Final Report, Charles Stark Draper Laboratory, Inc., Cambridge, Massachusetts.

[9] Li, D., and Vallery, H., 2012. "Gyroscopic assistance for human balance". In IEEE International Workshop on Advanced Motion Control.

[10] Matsuzaki, R., and Fujimoto, Y., 2013. "Walking assist device using control moment gyroscopes". In Proceedings of the IEEE Industrial Electronics Society Annual Conference (IECON).

[11] Leve, F. A., 2008. "Development of the spacecraft orientation buoyancy experimental kiosk". Master's thesis, University of Florida.

[12] Wojtara, T., Sasaki, M., Konosu, H., Yamashita, M., Shimoda, S., Alnajjar, F., and Kimura, H., 2012. "Artificial balancer - supporting device for postural reflex". *Gait & Posture,* ***35***, pp. 316–321.

[13] Winfree, K. N., Gewirtz, J. E., Mather, T., Fiene, J., and Kuchenbecker, K. J., 2009. "A high fidelity ungrounded torque feedback device: The iTorqU 2.0". In EuroHaptics Conference and Symposium on Haptic Interfaces for Virtual Environment and Teleoperator Systems.

[14] Yano, H., Yoshie, M., and Iwata, H., 2003. "Development of a non-grounded haptic interface using the gyro effect". In Proceedings of the 11th Symposium on Haptic Interfaces for Virtual Enviroment and Teleoperator Systems (HAPTICS).

[15] Badshah, A., Gupta, S., Morris, D., Patel, S., and Tan, D., 2012. "Gyrotab: A handheld device that provides reactive torque feedback". In Proceedings of the SIGCHI Conference on Human Factors in Computing Systems, pp. 3153–3156.

[16] Wie, B., 1998. *Space Vehicle Dynamics and Control*. AIAA.

[17] Lappas, V. J., 2002. "A control moment gyro (CMG) based attitude control system (ACS) for agile small satellites". PhD thesis, University of Surrey, Surrey, UK, October.

[18] Brown, D., and Peck, M. A., 2008. "Scissored-pair control-moment gyros: A mechanical constraint saves power". *Journal of Guidance, Control, and Dynamics,* ***31***(6), pp. 1823–1826.

[19] U.S. Department of Health and Human Services, 2012. Anthropometric reference data for children and adults: United states, 2007 - 2010. Vital and Health Statistics Series 11,

Copyright © 2014 by ASME

Number 252, Centers for Disease Control and Prevention.
[20] Tözeren, A., 1999. *Human Body Dynamics*. Springer-Verlag.
[21] Bourke, A. K., and Lyons, G. M., 2008. "A threshold-based fall-detection algorithm using a bi-axial gyroscope sensor". *Medical Engineering & Physics,* ***30***, pp. 84–90.
[22] Meuleman, J. H., Asseldonk, E. H., and Kooij, H., 2013. "The effect of directional inertias added to pelvis and ankle on gait". *Journal of NeuroEngineering and Rehabilitation,* ***10***(40), pp. 1–12.

Copyright © 2014 by ASME